arXiv:1410.2562v1 [physics.ao-ph] 9 Oct 2014

The Impact of Oceanic Heat Transport on the Atmospheric Circulation: a Thermodynamic Perspective

Alexander Schröder*, Valerio Lucarini† and Frank Lunkeit‡

Abstract

The present study investigates how global thermodynamic properties of the climate system are affected by the changes in the intensity of the imposed oceanic heat transport in an atmospheric general circulation model in aqua-planet configuration. Increasing the poleward oceanic heat transport results in an overall increase in the surface temperature and a decrease in the equator-to-pole surface temperature difference as a result of the ice-albedo feedback. Following the classical ansatz by Stone, the atmospheric heat transport changes in such a way that the total poleward heat transport remains almost unchanged. We also find that the efficiency of the climate machine, the intensity of the Lorenz energy cycle and the material entropy production of the system decline with increased oceanic heat transport which suggests that the climate system becomes less efficient and turns into a state of reduced entropy production, as the enhanced oceanic transport performs a stronger large-scale mixing between geophysical fluids with different temperature, thus reducing the availability in the climate system and bringing it closer to a state of thermal equilibrium.

*Email: alexander.schroeder@studium.uni-hamburg.de
Meteorologisches Institut, Klima Campus, University of Hamburg, Grindelberg 5, 20144 Hamburg
†Email: valerio.lucarini@uni-hamburg.de
Tel: +49 (0) 40 42838 9208
Meteorologisches Institut, Klima Campus, University of Hamburg, Grindelberg 7, 20144 Hamburg
Department of Mathematics and Statistics, University of Reading, Reading, RG6 6AX, UK
‡Email: frank.lunkeit@uni-hamburg.de
Phone: +49 (0) 40 42838 5073
Meteorologisches Institut, Klima Campus, University of Hamburg, Grindelberg 5, 20144 Hamburg

1 Introduction

The climate is a forced and dissipative non-equilibrium system, which, neglecting secular trends, can be considered in steady state, i.e. its statistical properties do not depend on time, and on the global scale, the energy and entropy budgets are closed. The positive budget of incoming over outgoing radiation at the top of the atmosphere in the tropical regions is compensated by a negative budget in the high latitudes. The large-scale geophysical fluids transport the excess of energy from low to high latitudes. The entropy budget is achieved in such a way that the sum of the integrated incoming entropy flux due to the solar high frequency photons plus the entropy generated by irreversible processes in the geophysical fluids and as a result of the the absorption and emission of photons are compensated by the radiation to space of low frequency photons. Most of the entropy production results from optical processes, while a smaller portion - referred to as material entropy production - is related to the irreversible processes in terms of the geophysical fluids (Kleidon and Lorenz, 2005). So the Earth is, in contrast to a system that is isolated and, therefore, maintaining a state of equilibrium, a thermodynamic system that exchanges energy and entropy with space (Ambaum, 2010).

The large-scale fluid climatic motions result from the conversion of available potential energy - due to the inhomogeneous absorption of solar radiation, with positive correlation between heating and temperature patterns - into kinetic energy, through instabilities coming, typically, from the presence of temperature gradients (Lorenz, 1955). Such instabilities tend to reduce the same temperature gradients they feed upon, by mixing fluid masses. The kinetic energy is then dissipated inside the system. In steady state conditions, the production of available potential energy, its conversion to kinetic energy, and the dissipation of kinetic energy have the same average rate, which corresponds to the intensity of the Lorenz (1955; 1967) energy cycle. The closure of such a thermodynamical/dynamical problem amounts to a self-consistent theory of climate.

Fuelled by the presence of temperature gradients, the climate system can be interpreted as a thermal engine that converts potential into mechanical energy (Peixoto and Oort, 1992). Recently, using tools of macroscopic nonequilibrium thermodynamics, a line has been drawn connecting a measure of the efficiency of the climate system, the spatio-temporal variability of its heating and temperature fields, the intensity of the Lorenz energy cycle, and the material entropy production (Johnson, 2000; Lucarini, 2009; Lucarini et al., 2011).

The role of oceanic heat transport in the climate system is a central aspect of climate dynamics and has drawn a great attention in the field of climate science. Herweijer et al.

(2005) observed that the presence of oceanic heat transport results into an overall warming of the surface. Barreiro et al. (2011) have shown that an increase in oceanic heat transport raises the global mean temperature by decreasing the albedo due to reduced sea-ice extent and marine stratus cloud cover and by increasing the greenhouse effect through a moistening of the atmosphere. Rose and Ferreira (2013) studied the role of oceanic heat transport with an idealised aqua-planet GCM. They focused on the problem of clarifying how oceanic heat transport affects the meridional surface temperature field.

Stone (1978) argued that the total poleward heat transport, defined as the sum of atmospheric and oceanic transport, is to a good approximation set by the planetary albedo and astronomical parameters. Stone states that the transport regime is weakly sensitive to the presence of oceans, mountains or the hydrological cycle, i.e. detailed atmospheric and oceanic processes that impact the transport mechanism. Experiments with coupled GCMs have shown an almost complete compensation by atmospheric heat transport for variations in oceanic heat transport (Manabe, 1969; Covey and Barron, 1988; Enderton and Marshall, 2009).

In the present study we explore the impact of the oceanic heat transport on macroscale thermodynamic quantities of the climate system. The aim is to characterise global nonequilibrium properties of the climatic machine in terms of their thermodynamical steady-state response to the change in the oceanic heat transport. Therefore, this work complements previous findings focusing on the investigation of the impacts of mean climate properties and circulation patters. We first look into the response of the meridional atmospheric heat transport, in order to test the hypothesis of ocean/atmosphere compensation, proposed in various forms by e.g. Bjerknes (1964) and Stone (1978). We then move from considering energy fluxes to looking at energy transformation, i.e. we investigate how changes in the ocean transport impact the intensity of the Lorenz (1955) energy cycle, and link this to changes in the spatio-temporal variability of the temperature in the atmosphere, by studying the properties of the effective warm and cold reservoirs constructed according to the theory proposed in Johnson (2000), Lucarini (2009) and Lucarini et al. (2010), so allowing the definition of a measure of the efficiency of the climate system. Finally, we will direct our attention to measuring the irreversibility of the climate system and study the impact of changing oceanic transport intensity on the material entropy production of the climate system. Our analysis tries to frame specific climatic processes of general relevance into a general physical framework, trying to advance the understanding of the climate as a non-equilibrium, forced and dissipative macroscopic system.

As a first step into this way of looking at the coupling between atmosphere and ocean, we consider a simplified yet physically relevant modelling set-up. We use a climate model of intermediate complexity, PlaSim (Fraedrich et al., 2005), which features a simplified yet reasonable representation of the 3D dynamics of the atmosphere and of its interactions with land and ocean boundary and surface layers. Instead, the representation of the ocean processes is severely simplified, as no explicit description of dynamic processes is given. The ocean rather provides prescribed lower boundary conditions (sensible and latent heat fluxes, albedo) for the atmosphere above. While this is an obvious limitation in terms of realism, such a setting allows for flexibly modulating the atmosphere/ocean interaction.

The paper is organized as follows. In section 2 we summarise the theoretical background on non-equilibrium thermodynamical properties of the climate system. In section 3 we describe the properties of the numerical model considered in this study and present the set of experiments we have performed. In section 4 we present the main results of our work. The summary of our findings and the related discussion are presented in section 5.

2 Theoretical framework

We wish to highlight two important aspects of the geophysical fluids of the climate system. First, they transport heat from regions featuring net positive energy budget at the top of the atmosphere (low latitudes) to regions where such budget is negative (high latitudes), thus reducing the temperature gradient between equator and poles (Peixoto and Oort, 1992; Lucarini and Ragone, 2011). Secondly, they perform on the average a net positive work due to the positive correlation between temperature and heating fields. Such work is used to uphold the kinetic energy of the global circulation against the frictional dissipation (Peixoto and Oort, 1992). The general circulation of the atmospheric system arises from the conversion of available potential energy into kinetic energy (e.g. atmospheric motions), as introduced in the formulation of the energy cycle in Lorenz (1955, 1967). If the climate system is at statistical steady state, the rate of generation of available potential energy $\dot{G}$, the rate of conversion of potential into kinetic energy $\dot{W}$, and the dissipation rate of kinetic energy $\dot{D}$ are equal when averaged over a long period of time (e.g. several years), so that $\overline{\dot{G}} = \overline{\dot{W}} = \overline{\dot{D}} > 0$, where the bar indicates the operation of time averaging. This allows for characterising the strength of the Lorenz energy cycle in several ways. Let us briefly recapitulate, following Johnson (2000) and

Lucarini (2009), some thermodynamic ideas we will use throughout the paper.

Let Ω be the volume domain of the climate system and $\dot{Q}$ be the local heating rate due to frictional dissipation and convergence of heat fluxes including radiative, sensible and latent heat components. At each instant t we divide Ω into two subsections, so that $Q(x,t) > 0$, $x \in \Omega^+$ defining Q^+, and $Q(x,t) < 0$, $x \in \Omega^-$ for Q^- respectively. We wish to remark that the domains Ω^+ and Ω^- are time dependent. Integrating the two heating components results in: $\int_{\Omega^+} \rho \dot{Q}^+ \mathrm{d}V + \int_{\Omega^-} \rho \dot{Q}^- \mathrm{d}V = \dot{\Phi}^+ + \dot{\Phi}^-$. Johnson (2000) and Lucarini (2009) show that the time average $\overline{\dot{\Phi}^+} + \overline{\dot{\Phi}^-}$ gives the rate of generation of available potential energy, so that:

$$\overline{\dot{W}} = \overline{\dot{\Phi}^+} + \overline{\dot{\Phi}^-}. \tag{1}$$

The efficiency of the climate machine can now be expressed as:

$$\eta = \frac{\overline{\dot{\Phi}^+} + \overline{\dot{\Phi}^-}}{\overline{\dot{\Phi}^+}}. \tag{2}$$

This expression represents the ratio for the work output $\overline{\dot{\Phi}^+} + \overline{\dot{\Phi}^-}$ to the heat input $\overline{\dot{\Phi}^+}$. At each instant one defines the quantities $\Sigma^{+(-)} = \int_{\Omega}^{+(-)} \rho \dot{Q}^{+(-)} / T$, which are the instantaneous entropy sources and sinks in the system. As explained in Johnson (2000) and Lucarini (2009), we have that $\overline{\dot{\Sigma}^+} + \overline{\dot{\Sigma}^-} = 0$. We can then introduce the scale temperatures $\Theta^+ = \overline{\dot{\Phi}^+} / \overline{\dot{\Sigma}^+}$ and $\Theta^- = \overline{\dot{\Phi}^-} / \overline{\dot{\Sigma}^-}$, so that equation 2 can be rewritten as $\eta = \frac{\Theta^+ - \Theta^-}{\Theta^+}$, where $\Theta^+ > \Theta^-$.

Hence, the motion of the general circulation of the system can be sustained against friction because zones being already relatively warm absorb heat whereas the relatively low temperature zones are cooled.

The Lorenz energy cycle can thus be seen as resulting from the work of an equivalent Carnot engine operating between the two (dynamically determined) reservoirs at temperature Θ^+ and Θ^-. Yet, the climate is far from being a perfect engine, as many irreversible processes take place; nonetheless, a Carnot-equivalent picture can be drawn as described.

Let us now delve into such irreversible processes. In the climate system two rather different sets of processes contribute to the total entropy production (Peixoto and Oort, 1992; Goody, 2000; Ambaum, 2010). The first set of processes is responsible for the irreversible thermalisation of photons emitted near the Sun's corona at roughly 5800 K, absorbed and then re-emitted at much lower temperatures, typical of the Earth's climate ($\sim$255 K). This gives the largest contribution to the total average rate of entropy

production for the Earth system of about $900\,\mathrm{mW\,m^{-2}\,K^{-1}}$ (Peixoto and Oort, 1992; Ambaum, 2010). The remaining contribution is due to the processes responsible for mixing and diffusion inside the fluid component of the Earth system, and for the dissipation of kinetic energy due to viscous processes. This constitutes the so-called material entropy production, and is considered to be the entropy related quantity of main interest as far as the properties of the climate system are concerned. Further relevant research on entropy production in the climate system treating also the geochemical and radiative contribution to entropy production can be found in Kleidon (2009) and Wu and Liu (2010) respectively.

The entropy budget of geophysical fluids at steady state, following Goody (2000); Lucarini et al. (2011), is given by:

$$\overline{\dot{S}(\Omega)} = \int_{\Omega} \rho \left(\overline{\frac{\dot{q}_{rad}}{T}} + \overline{\dot{s}_{mat}} \right) \mathrm{d}V = 0, \tag{3}$$

where $\dot{q}_{rad}$ indicates the heating rate by the convergence of radiative fluxes, T is the local temperature at which the energy is gained or lost, while $\dot{s}_{mat}$ represents the density of entropy production associated with the irreversibility of processes involving the fluid medium. Equation 3 represents the entropy budget and states that in a steady state the radiative entropy source must be balanced by the rate of material entropy production $\dot{S}_{mat}$ due to material irreversible processes. See a detailed discussion of this aspect in Lucarini and Pascale (2014), where the contributions to the material entropy production at various spatial and temporal scales are discussed.

In a steady-state climate the material entropy production $\dot{S}_{mat}(\Omega)$ can be expressed in general terms as:

$$\overline{\dot{S}_{\mathrm{mat}}(\Omega)} = \int_{\Omega} \rho \overline{\dot{s}_{mat}} \mathrm{d}V = \int_{\Omega} \overline{\frac{\varepsilon^2}{T}} \mathrm{d}V + \int_{\Omega} \overline{(\vec{F}_{sens} + \vec{F}_{lat}) \cdot \vec{\nabla} \frac{1}{T}} \mathrm{d}V = - \int_{\Omega} \rho \overline{\frac{\dot{q}_{rad}}{T}} \mathrm{d}V, \tag{4}$$

where $\overline{\dot{s}_{mat}}$ is the time averaged density of entropy production due to the following irreversible processes inside the medium: dissipation of kinetic energy (ε^2 is the specific dissipation rate) and turbulent transport of heat down the temperature gradient ($\vec{F}_{sens}$ and $\vec{F}_{lat}$, being the sensible and latent turbulent heat fluxes, respectively).

One needs to underline that a more refined treatment of the entropy production related to the hydrological cycle has been proposed by e.g. Pauluis and Held (2002a), Pauluis and Held (2002b) and Romps (2008). Nonetheless, as discussed in Lucarini et al. (2014), the overall contribution of the entropy production due to the hydrological cycle

can be reconstructed to a high degree of accuracy also in the simplified method proposed here.

Note that one can compute the entropy production as:

$$\overline{\dot{S}_{\mathrm{mat}}(\Omega)} = \int_{\Omega} \frac{\overline{\varepsilon^2}}{T} \mathrm{d}V + \int_{\Omega} \frac{\overline{-\vec{\nabla}\cdot(\vec{F}_{sens} + \vec{F}_{lat})}}{T} \mathrm{d}V + \int_{\partial\Omega} \frac{\overline{\vec{F}_{sens} + \vec{F}_{lat}}}{T} \cdot \hat{n} \mathrm{d}S, \tag{5}$$

where the first term is unchanged, the second terms describes the entropy gain and loss due to heating and cooling by convergence of sensible and latent heat fluxes, and the last term is the net entropy flux across the boundaries of Ω. If one consider the atmospheric domain as Ω, such term becomes equal to the integral at surface of the ratio between the sum of the sensible and of the latent heat flux divided by the surface temperature. Equation 5 represents the way entropy production is typically computed in numerical models. If one considers the whole climate system as Ω, the boundary terms disappear. Nonetheless, another term proportional to a Dirac's delta at $z = z_{surf} = 0$ appears, resulting from the divergence of the turbulent flux due to the net evaporation at surface. If we integrate over Ω, the contribution of this term is exactly the same as in the case where Ω corresponds to the atmosphere only. In other terms, our simplified representation of the ocean is such that all the entropy is produced in the atmosphere.

We can now separate in equation 4 - or, equivalently, in equation 5 the first term from the rest, so that, following Lucarini (2009), the material entropy production can be expressed as:

$$\overline{\dot{S}_{mat}(\Omega)} = \overline{\dot{S}_{min}(\Omega)} + \overline{\dot{S}_{exc}(\Omega)}, \tag{6}$$

where $\overline{\dot{S}_{min}(\Omega)}$ is the minimum value of entropy production compatible with the presence of average dissipation rate $\int_{\Omega} \epsilon^2 \mathrm{d}V$, while $\overline{\dot{S}_{exc}(\Omega)}$ is the excess of entropy production with respect to such minimum. One can associate $\overline{\dot{S}_{min}}$ exactly with the term in equation 4 related to the dissipation of kinetic energy, while $\overline{\dot{S}_{exc}}$ can be identified with the sum of the other two terms.

If we take the ratio of the two terms on the right-hand side in equation 6, we have that.

$$\alpha = \frac{\overline{\dot{S}_{exc}(\Omega)}}{\overline{\dot{S}_{min}(\Omega)}} \approx \frac{\int_{\Omega} \overline{(\vec{F}_{sens} + \vec{F}_{lat}) \cdot \vec{\nabla} \frac{1}{T}} \mathrm{d}V}{\int_{\Omega} \frac{\overline{\varepsilon^2}}{T} \mathrm{d}V}, \tag{7}$$

where α is the degree of irreversibility (Lucarini, 2009) and determines the ratio between the contributions to entropy production by down-gradient turbulent transport and by viscous dissipation of mechanical energy. If this ratio is close to zero ($\alpha \to 0$),

all the production of entropy is exclusively caused by unavoidable viscous dissipation. Pursuing this further, if the turbulent heat transport in the system from high to low temperature regions is enhanced, then entropy production is also increased. However, if the turbulent heat transport down the temperature gradient is maximised, the efficiency declines due to the reduction of the temperature difference between the warm and cold reservoir.

3 Experimental design

The Planet Simulator (PlaSim; Fraedrich et al., 2005), a climate model of intermediate complexity and freely available at www.mi.uni-hamburg.de/plasim, is applied and used within an idealised aqua-planet configuration. PlaSim consists of a dynamical core that solves primitive equations numerically. Unresolved processes are parametrised for: long- and short-wave radiation (Sasamori, 1968; Lacis and Hansen, 1974), moist (Kuo, 1965) and dry convection, cloud formation (Stephens, 1978, 1984; Slingo and Slingo, 1991) and large-scale precipitation, latent and sensible heat boundary layer fluxes, horizontal and vertical diffusion (Louis, 1979; Laursen and Eliasen, 1989; Roeckner et al., 1992).

The main goal of this work is to study the sensitivity of the nonequilibrium thermodynamical properties of the climate to the intensity of the oceanic heat transfer. Inspired by Rose and Ferreira (2013), we have performed climate simulations in which the oceanic heat transport can be parametrically modulated. Peaks of the oceanic heat flux range from 0.0 PW over present-day value, which is roughly 1.0 PW - 2.0 PW (Trenberth and Caron, 2001), up to 4.0 PW.

The setup includes a global slab ocean with a 60 m mixed-layer including a thermodynamic sea-ice model. Oceanic heat transport is controlled by a simple analytical expression to be explained below. The astrophysical parameters are adjusted to present-day values for planet Earth except that eccentricity is set to zero.

The series of experiments is performed in a setup of 5 vertical layers and T 31 spectral resolution, corresponding to a Gaussian grid resolution of about $3.75° \times 3.75°$. This particular setup is an extreme simplification. However, basic physical elements crucial for simulating climate features are retained following Rose and Ferreira, 2013. The analytical function used to control the prescribed oceanic heat transport Ψ as a function of geographical latitude ϕ is

$$\Psi(\phi) = \Psi_{\text{amp}} \sin(\phi) \cos^{2N}(\phi), \tag{8}$$

where Ψ_{amp} is the amplitude in units of PW and N is the scale parameter, which is

held constant by the value $N = 2$ for all simulations. $\Psi_{\max}$ is the peak oceanic heat transport and $\phi_{\max}$ is the latitude at which the oceanic heat transport Ψ reaches a maximum. For $N = 2$ the poleward transport is maximised at about 27° N/S.

Each simulation is performed using a different value of $\Psi_{\max}$ which varies between 0.0 PW (control run) to 4.0 PW with an increment of 0.5 PW, i.e. $\Psi_{\max} = \{0.0, 0.5, ..., 4.0\}$ PW.

The oceanic heat transport and its convergence, the so-called q-flux (Rose and Ferreira, 2013), which determines the oceanic heat transport, are displayed in figure 1(a). The q-flux implemented in the model is given the characteristics of being zonally symmetric and steady in time for all simulations. As shown in figure 1(b), the q-flux is negative in the tropics (heat uptake into the ocean) and positive in the mid and high latitudes (heat release into the atmosphere). As a consequence of the heat uptake and release at the ocean's surface, there is a maximum transport of heat just in between those regions of heat absorption and release, as displayed in figure 1(a).

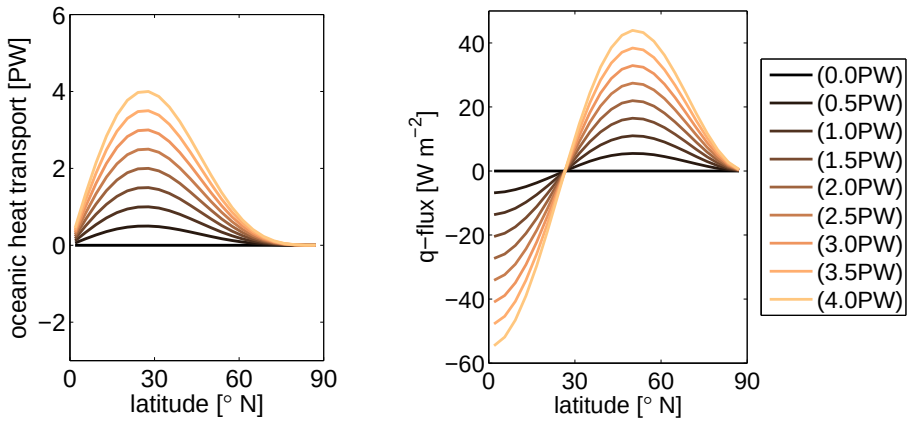

Figure 1: Oceanic heat transport (a) and q-flux (b) as a function of latitude for all simulations.

Each model run consists of 100 years to ensure the final 30 years, that are used for diagnostics, are free from any influence of the model's transient phase at the beginning of each run.

4 Results

We study the atmospheric response in the meridional heat transport for different scenarios of the q-flux in figure 2(a) by looking into the time-averaged and vertically integ-

rated zonal mean transport of moist static energy.

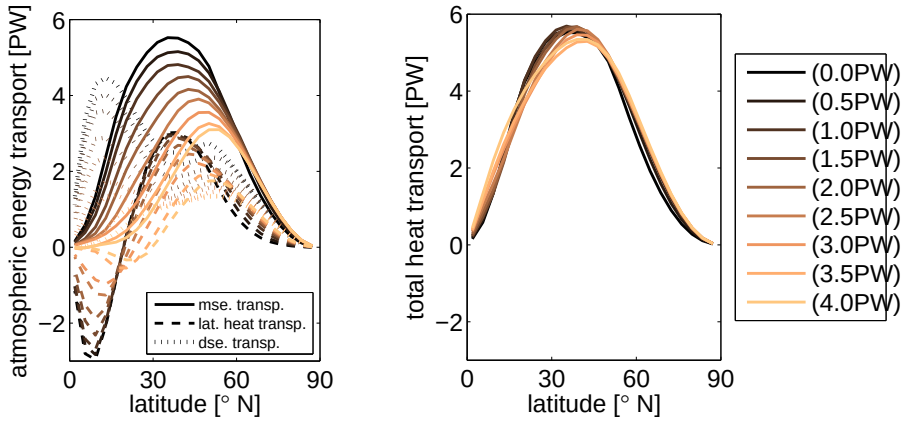

Figure 2: Time-averaged meridional moist static energy transport (mse. transp.) with latent heat transport (lat. heat transp.) and dry static energy transport (dse. transp.) (a), and the total energy transport (b) as oceanic heat transport is increased.

As well known, the geophysical fluids transport energy from the low to the high latitude regions, the effect being that the meridional temperature gradient decreases and entropy is produced (Peixoto and Oort, 1992; Ozawa et al., 2003). We find that the peak amplitude of the atmospheric energy transport decreases linearly with the value of the peak oceanic energy transport $\Psi_{\max}$. For every 0.5 PW increase in oceanic energy transport peak $\Psi_{\max}$, the maximum intensity of the atmospheric energy transport decreases by about 0.3 PW. When increasing the peak oceanic heat transport from $\Psi_{\max} = 0.0$ PW to $\Psi_{\max} = 4.0$ PW, we observe a latitudinal relocation of the peak atmospheric heat flux from 35° to 53°, with the effect of shifting the maximum of the baroclinic activity. As a consequence of the latitudinal shift as well as the decrease in the maximum intensity, the atmospheric heat transport features a decrease in the tropics and subtropics because here the oceanic transport is increased and thus dominates the total transfer out of the tropics. The strongest changes in the latitudinal profile of the atmospheric transport take place in the low and mid latitudes. Between 16° and 28° N/S deviations in atmospheric heat transport from the control run are largest.

The total meridional energy transport, which is computed as the sum of oceanic and atmospheric energy transport, is almost unchanged for increased $\Psi_{\max}$ (see figure 2(b)). This result confirms the statement in Stone (1978) about the insensitivity of the magnitude of the total transport to internal parameters (e.g. meridional temperature gradient). Outgoing longwave radiation balances the changes in absorbed short-wave

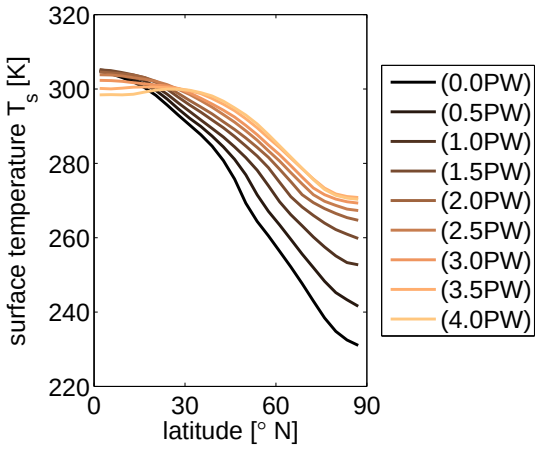

Figure 3: Meridional time-averaged surface temperature profile as a function of oceanic heat transport.

radiation, so that as a result, the net radiative forcing at top of the atmosphere is roughly unchanged. Similar results have been presented in Rose and Ferreira (2013).

Surface temperature is indeed a quantity of fundamental interest for climate studies. Figure 3 shows the time-averaged zonal mean surface temperature profile with increased oceanic heat transport. The equator-to-pole temperature gradient $\Delta T = T_{s,eq} - T_{s,pole}$ is larger than 70 K in the control run. This gradient largely decreases as oceanic heat transport increases. On average ΔT declines by 5.5 K for every 0.5 PW increase in $\Psi_{\max}$. The gradient reduction is mainly due to a temperature increase at the poles, except for oceanic heat transport larger than 2.5 PW at which the temperature decrease at the equator becomes more relevant.

We note a temperature maximum in the subtropics on both hemispheres for the runs with $\Psi_{\max} = 3.5$ PW and $\Psi_{\max} = 4.0$ PW, where a small reversed temperature gradient between the deep tropics and subtropics develops.

The time average of the global mean temperature at the surface T_s features a positive sensitivity on the increased $\Psi_{\max}$ (see figure 4). The climate system features a global warming at the surface of roughly 10 K for the whole range of $\Psi_{\max}$. This is because increased near-surface heat transport in the northern regions reduces the sea-ice extent which feeds into the positive ice-albedo feedback, with the ensuing increase of the global surface temperature.

Let's now shift our attention to the two quantities Θ^+ and Θ^-, which characterise the warm and cold reservoirs of the climate engine. Qualitatively, the two temperatures behave similarly when $\Psi_{\max}$ is changed. We can classify three temperature regimes:

i) $\Psi_{\max} < 2.0\,\mathrm{PW}$ atmospheric warming, ii) $2.0\,\mathrm{PW} \leq \Psi_{\max} \leq 3.5\,\mathrm{PW}$ atmospheric cooling, and iii) $\Psi_{\max} > 3.5\,\mathrm{PW}$ weak sensitivity. We observe a higher sensitivity of Θ^- than Θ^+ for i) which is generally due to the amplified polar warming. The difference between Θ^+ and Θ^-, denoted as $\Delta\Theta$, decreases with increasing $\Psi_{\max}$. We now try to find a rationale of why increases in the imposed oceanic heat transport cause a reduction of the temperature difference between the warm and cold reservoir, thereby implying a decrease in the atmospheric efficiency of the climate engine. Interestingly, the difference between T_s and the average of Θ^- and Θ^+ increases with $\Psi_{\max}$, especially for $\Psi_{\max} \leq 3.0\,\mathrm{PW}$, indicating a reduction in the stability of the atmosphere. This is understood by considering that larger oceanic transports lead to stronger warming at low levels in the mid and high latitudes, which, as suggested by figure 2, must be compensated by a weaker heat transport aloft.

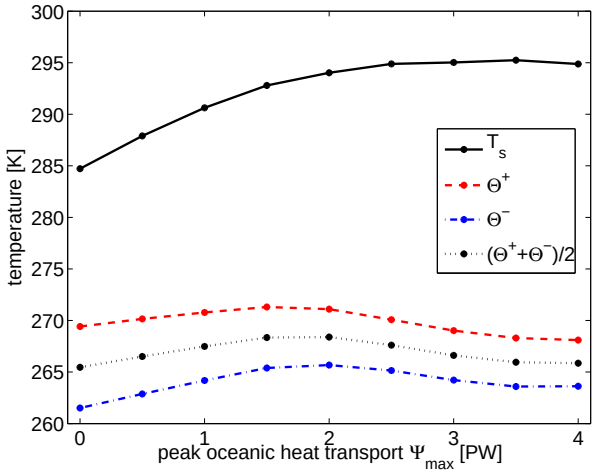

Figure 4: Time average of the global mean surface temperature T_s and of the temperature of the warm (Θ^+) and the cold (Θ^-) pool.

The diabatic heating processes constitute the sources and sinks of internal energy for the atmosphere and play a decisive role in the generation and destruction of available potential energy (Peixoto and Oort, 1992). Those processes are displayed as the time- and zonal-averaged diabatic heating rates $^{dT_a}/_{dt}$ (see figure 5). The heating rate is calculated as the sum over all diabatic heating effects including heating or cooling by the response of radiative heat fluxes, sensible and latent heat fluxes and vertical diffusion. While Θ^+ and Θ^- are defined using the time and space dependent heating fields, as described above, inspecting the time and zonal averages of the heating patterns is useful for understanding how available potential energy is generated.

Simulations with $0.5\,\mathrm{PW} \leq \Psi_{\max} \leq 1.5\,\mathrm{PW}$ show diabatic warming in the deep tropics in the mid troposphere and in the subtropical low troposphere, whereas diabatic cooling occurs in the mid and high troposphere of the subtropics and in polar as well as subpolar regions. Positive heating in the tropical and subtropical regions is dominated by the contribution of latent heat fluxes, in particular, heating through convective precipitation (not shown here). In the mid to high latitude regions large-scale precipitation contributes towards a positive heating. Diabatic cooling, on the other hand, is mostly caused by outgoing longwave radiation and to a moderate extent by the conversion process from rain to snow mostly in the subtropical regions.

We see an extension of the area of positive heating in the mid latitudes towards the poles in the lower troposphere as well as in the equatorial mid and upper troposphere for larger values of $\Psi_{\max}$. The poleward migration of the positive heating pattern in the mid-latitudes is closely related to the poleward shift of the atmospheric latent heat transport. The area of positive heating broadens in height at latitudes around 50°. Since the positive heating patterns (relevant for defining Θ^+) in the mid latitudes extend in height and is, in addition, stretched poleward, lower temperatures are considered in the quantity of Θ^+, which explains the smaller sensitivity of Θ^+ than of Θ^- for $0.0\,\mathrm{PW} \leq \Psi_{\max} \leq 1.5\,\mathrm{PW}$ in figure 4. By implication, the warming effect at polar latitudes causes the sensitivity of Θ^- to be larger than of Θ^+. For $\Psi_{\max} \geq 2.0\,\mathrm{PW}$ the sensitivity of both, Θ^+ and Θ^-, is negative since large parts of the tropical high and mid troposphere cools.

We observe on average a decline in $\Delta\Theta = \Theta^+ - \Theta^-$ of approximately $0.4\,\mathrm{K}$ for every $0.5\,\mathrm{PW}$ increase in $\Psi_{\max}$ (figure 6(a); green graph). The total temperature difference decreases from $7.9\,\mathrm{K}$ to $4.5\,\mathrm{K}$ across the considered range of values of $\Psi_{\max}$. The climate system becomes horizontally more isothermal as $\Psi_{\max}$ is reinforced, which is consistent with the decline for the meridional difference in surface temperature $\Delta T = T_{s,eq} - T_{s,pole}$ (figure 6(a); blue graph). We find an accurate linear relation between ΔT and $\Delta\Theta$ (the temperature difference between the two thermal reservoirs, Θ^- and Θ^+): for every observed $10\,\mathrm{K}$ decline in ΔT the temperature difference, $\Delta\Theta$, decreases linearly by approximately $0.8\,\mathrm{K}$ on average, as shown in figure 6(b). This provides a potentially interesting indication of how to relate changes in the surface temperature gradient to quantities describing the dynamic processes in the atmosphere.

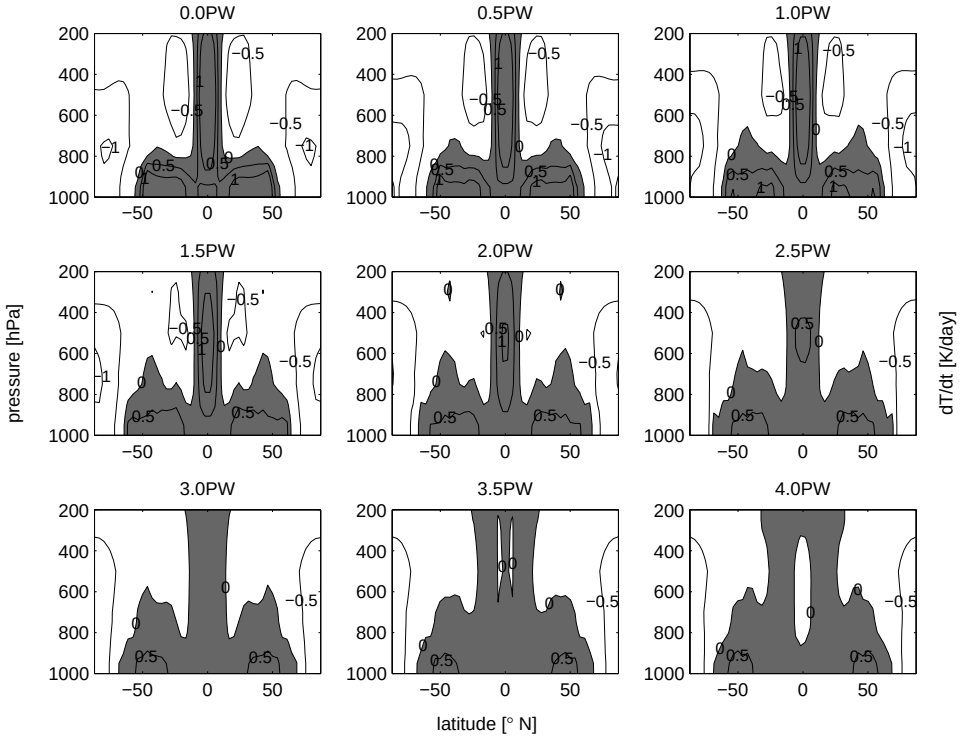

Figure 5: Zonally averaged mean heating rates in the atmosphere for oceanic heat transport ranging from 0.0 PW (upper left panel) to 4.0 PW (low right panel), where grey-shaded areas indicate positive and white areas negative heating rates in $[\mathrm{K/day}]$.

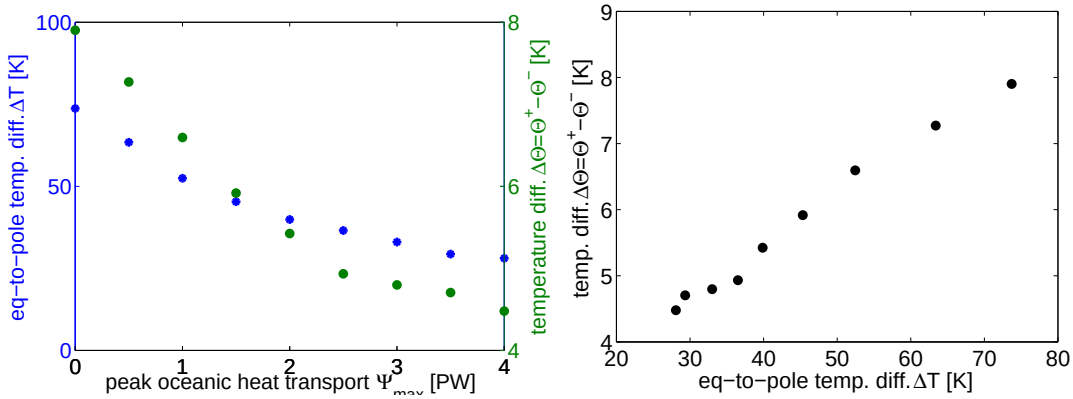

Figure 6: Scatter plot of time-averaged global mean temperature difference between equator and pole (blue) as well as Θ^+ and Θ^- (green) as a function of maximum energy transport in the ocean (a). Scatter plot of time-averaged global mean temperature difference between equator and pole as well as Θ^+ and Θ^- (b).

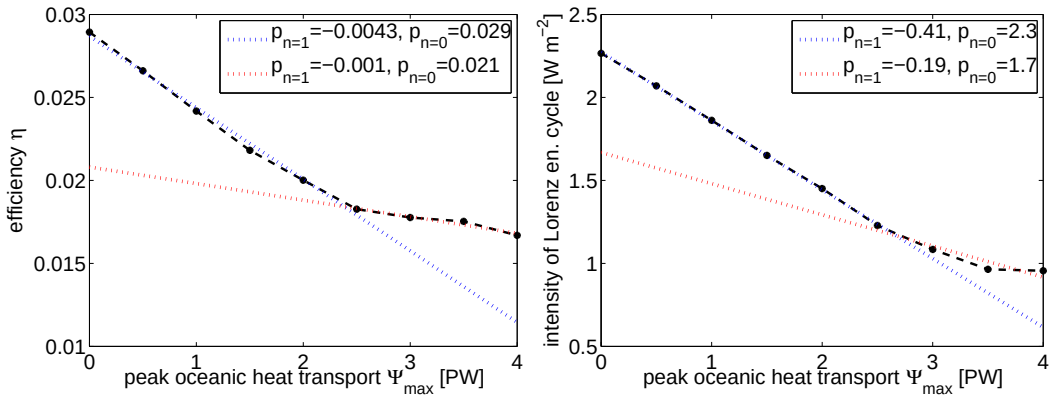

Figure 7: Time average of efficiency η (a) and intensity of the Lorenz energy cycle $\overline{\dot{W}}$ (b) for steady state obtained for varying oceanic heat transport. Dotted line represents best linear fit for i) $0.0\,\mathrm{PW} \leq \Psi_{\max} \leq 2.5\,\mathrm{PW}$ (blue) and for ii) $2.5\,\mathrm{PW} \leq \Psi_{\max} \leq 4.0\,\mathrm{PW}$ (red) with polynomial coefficients of n-th order, $\mathrm{p_{n=1}}$ and $\mathrm{p_{n=0}}$.

As the climate warms and the temperature difference between the warm and the cold reservoir shrinks with increased $\Psi_{\max}$, the efficiency η and the intensity of the Lorenz energy cycle $\overline{\dot{W}}$ of the climate system decline (see figure 7). The increase in $\Psi_{\max}$ causes the climatic machine to act less efficient, in terms of a decrease of the ratio between mechanical energy output and thermal energy input.

Figure 7 shows η and $\overline{\dot{W}}$. We observe a remarkably linear behaviour for both quantities when considering the first 6 runs with $0.0\,\mathrm{PW} \leq \Psi_{\max} \leq 2.5\,\mathrm{PW}$. For every $0.5\,\mathrm{PW}$ increase in $\Psi_{\max}$ the efficiency η declines by about $2.0 \cdot 10^{-3}$, while the strength of Lorenz energy cycle $\overline{\dot{W}}$ decreases by about $0.2\,\mathrm{Wm^{-2}}$ (see dotted, blue graph in figure 7). For $\Psi_{\max}$ larger than present-day values ($\Psi_{\max} \leq 2.5$), η decreases by only $0.5 \cdot 10^{-3}$ per $0.5\,\mathrm{PW}$ increase, while $\overline{\dot{W}}$ declines by $0.1\,\mathrm{Wm^{-2}}$ per $0.5\,\mathrm{PW}$ increase (see dotted, red graph in figure 7). We observe an abrupt change in the tendency for $\Psi_{\max} = 2.5$; at which pronounced tropical and subtropical atmospheric cooling sets in. This indicates that the change in the temperature difference between equatorial and tropical regions cause a drastic change in the dynamical properties of the system.

The reason for this enhanced decrease in $\overline{\dot{W}}$ can be found in the decrease of the temperature difference between the warm and the cold reservoir. From energy conservation we know, the decrease in the strength of Lorenz energy cycle $\overline{\dot{W}}$ implies that also the total dissipation $\overline{\dot{D}}$ decreases in a steady state climate, as the climatic engine has smaller rate of transformation of available into kinetic energy. The decrease of $\overline{\dot{D}}$ implies, e.g.

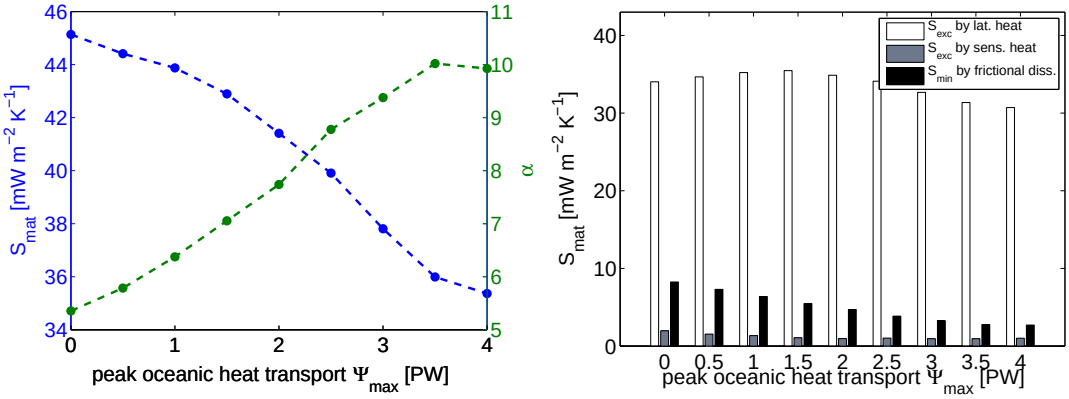

Figure 8: In (a) steady-state global mean material entropy production $\overline{\dot{S}_{mat}}$ (blue graph) and degree of irreversibility α, and in (b) most relevant contributions of $\overline{\dot{S}_{mat}}$ split into $\overline{\dot{S}_{exc}}$ and $\overline{\dot{S}_{min}}$, as a function of increasing oceanic heat transport.

that surface winds are weaker, because this is where most of the dissipation takes place. We note that by increasing $\Psi_{\max}$, warm and cold air masses get mixed more effectively with the result that the atmosphere becomes horizontally more isothermal and, hence, the climatic engine acts less efficiently.

Material entropy production $\overline{\dot{S}_{mat}}$, introduced in equation 4, as well as the degree of irreversibility α, introduced in equation 7, are shown in figure 8(a). With increasing values of $\Psi_{\max}$, the decrease in the intensity of the Lorenz energy cycle and the increase in the surface temperature imply a reduction of the part in $\overline{\dot{S}_{mat}}$ linked with frictional dissipation, which is related to lower bound of entropy production $\overline{\dot{S}_{min}}$. Nonetheless, one needs to investigate the excess of entropy production $\overline{\dot{S}_{exc}}$, which is linked to the turbulent heat fluxes down the temperature gradient. The relative decrease in entropy production due to frictional dissipation ($\overline{\dot{S}_{min}}$) is stronger than the relative decrease in entropy production by down-gradient turbulent heat transport ($\overline{\dot{S}_{exc}}$) as featured by the overall increase in α (figure 8(a)). Thus, the entropy production due to the turbulent heat transport down the gradient of the temperature field becomes more and more dominant as the oceanic transport increases because irreversible mixing becomes stronger. As a result the degree of irreversibility increases since larger oceanic heat transport implies larger mixing which impels $\overline{\dot{S}_{exc}}$.

In figure 8(b) the main contributions of the material entropy production in the model are displayed. This includes the contributive processes due to latent and sensible turbulent heat fluxes and frictional dissipation of kinetic energy. Entropy production by latent heat, including convective as well as large-scale precipitation, surface latent heat fluxes

and rain-snow conversion processes, makes by far the largest portion of material entropy production. For small intensities of $\Psi_{\max}$, the value of entropy production by latent heat reads $35\,\mathrm{mW\,m^{-2}\,K^{-1}}$. For increasing $\Psi_{\max}$ up to 1.5 PW the value increases by $2\,\mathrm{mW\,m^{-2}\,K^{-1}}$, while for larger values of $\Psi_{\max}$, this contribution to entropy production declines by $4\,\mathrm{mW\,m^{-2}\,K^{-1}}$. Entropy production by frictional dissipation decreases, as one would expect since dissipation is proportional to the intensity of the Lorenz energy cycle (shown in figure 7(b)). It decreases from $8\,\mathrm{mW\,m^{-2}\,K^{-1}}$ for $\Psi_{\max} = 0\,\mathrm{PW}$ down to $3\,\mathrm{mW\,m^{-2}\,K^{-1}}$ for $\Psi_{\max} = 4\,\mathrm{PW}$. Entropy production by sensible turbulent heat flux at the surface as well as in the atmosphere decreases by half (from $2\,\mathrm{mW\,m^{-2}\,K^{-1}}$ to $1\,\mathrm{mW\,m^{-2}\,K^{-1}}$) with $\Psi_{\max}$ increasing. One would expect that larger values of $\Psi_{\max}$ would lead to larger values of $\overline{\dot{S}_{mat}}$, using the argument that a warmer planet should be able to have a stronger hydrological cycle. For low values of $\Psi_{\max}$, the increase in $\overline{\dot{S}_{mat}}$ due to the hydrological cycle is overcompensated by the decrease in the contribution due to the frictional dissipation.

In order to further clarify the impacts on the material entropy production of increasing $\Psi_{\max}$, we split the material entropy production due to irreversible latent turbulent heat processes into the contributions coming from convective precipitation, large-scale precipitation, surface latent heat fluxes, and heat release by rain-snow conversion. Figure 9(a)-9(d) displays the time and zonal mean of these 4 contributions, where the process implicating convective precipitation gives the largest contribution, particularly in the tropics and subtropics, where most of atmospheric convection processes takes place. Note that the divergence of the horizontal turbulent latent and sensible heat fluxes divided by the local temperature, which correspond to the boundary part in equation 4 (the other being the surface fluxes of latent heat) are negligible.

We observe that the peak at the equator is significantly reduced, while convection processes move into the mid-latitudes for increased $\Psi_{\max}$ where the surfaced is heated and static stability decreases. Large-scale precipitation features are shifted out of the mid-latitudes towards higher latitudes. As large-scale precipitation regimes experience a shift to higher latitudes, their maximum intensity is almost kept constant. For the control run, latent heat fluxes at the surface show a maximum at latitudes of 20° to 25°. These maxima on both hemispheres indicate the region with maximum evaporation. As the heat transport in the ocean is increased, latent turbulent heat fluxes reduces largely in tropical and subtropical regions, and peak latent heat fluxes move towards mid-latitudes. The region with largest evaporation at the surface shifts from the subtropics to the mid-latitudes with increasing $\Psi_{\max}$. Atmospheric latent heat release by rain-snow conversion qualitatively shows, as expected due to high atmospheric processes, similar patterns as

the meridional profile for convective processes. Tropical regions are characterised by a considerable reduction of heat release, whereas the subtropics and mid-latitudes gain heat due to rain-snow conversion.

The material entropy production is negative in the tropical latitudinal band (figure 9(e)). This, of course, is perfectly compatible with the second law of thermodynamics and results from the fact that there is a net large scale transport of energy from those regions to the equator and to the mid latitudes as result of net moisture transport (figure 2(a)). Such a negative contribution is overcompensated by the positive material entropy production associate to the absorption of the transported latent heat.

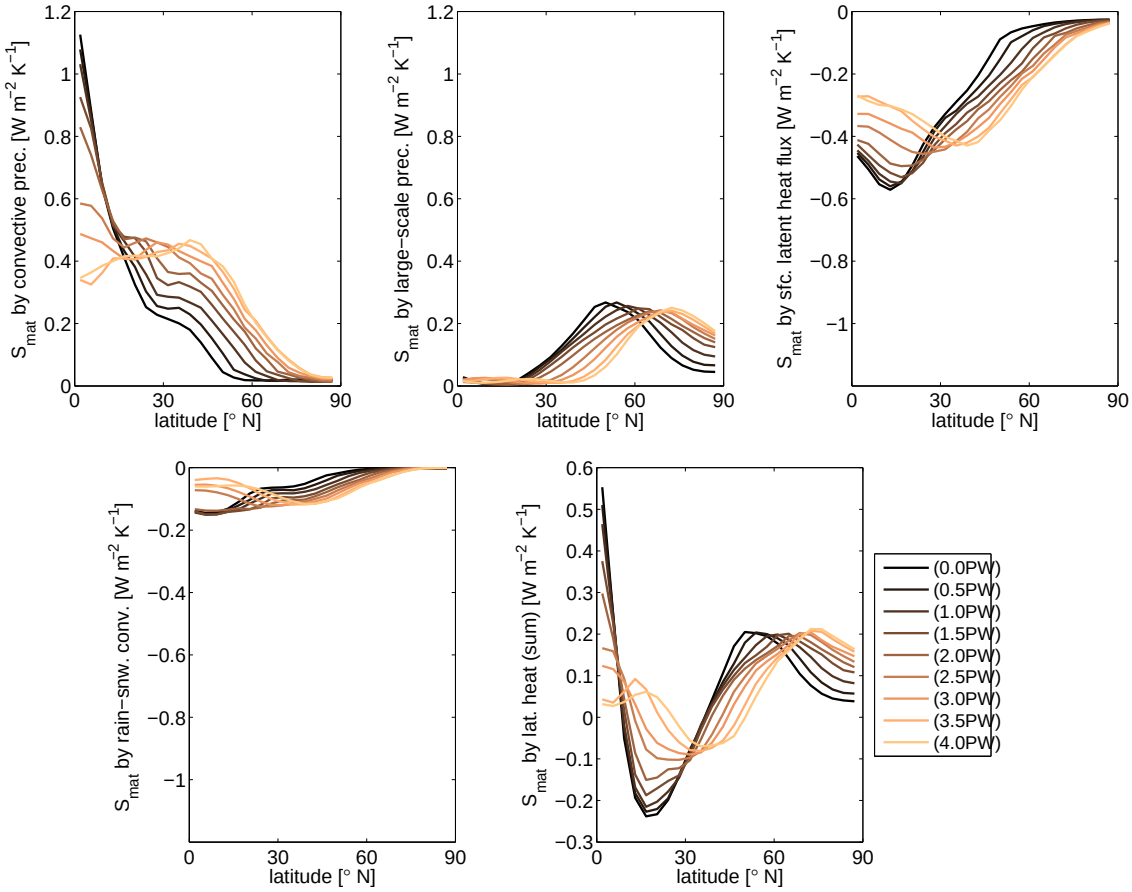

Figure 9: Time averaged zonal mean of 4 contributions of material entropy production concerning latent heat processes as a function of increasing oceanic heat transport. Material entropy production by convective precipitation (a); by large-scale precipitation (b); by surface latent heat fluxes (c); by rain-snow conversion (d). Sum of these 4 contributions (e).

5 Conclusions

In this investigation we have studied the climate sensitivity to changes in the ocean heat transport describing the response of macroscale thermodynamical properties of the climate system, coming from a theoretical framework introduced by Lucarini (2009). Stone (1978) states a full oceanic-atmospheric compensation, so that the total heat transport, as the sum of the oceanic and the atmospheric component, is insensitive to internal parameters of the atmosphere-ocean system, e.g. the meridional temperature gradient.

Our results show an almost exact compensation of the meridional heat transport in the atmosphere for increasing the meridional oceanic heat transport,$\Psi_{\max}$, from 0.0 PW to 4.0 PW by 0.5 PW. As a result, the total heat transport is almost insensitive to the direct impact of increasing the oceanic heat flux following Stone (1978). Minor deviations are assumed to stem from an altered planetary albedo due to a retreat in sea ice at the poles and a relocation of cloud formations.

Two major features in temperature properties of the climate system on the increase of meridional heat transport ($\Psi_{\max} = 0.0\,\mathrm{PW} \rightarrow \Psi_{\max} = 4.0\,\mathrm{PW}$) in the ocean can be noted: i) an increase in global mean surface temperature T_s of 10 K; ii) the reduction in the difference between the warm pool temperature Θ^+ and the cold pool temperature Θ^-. The latter implies that the atmospheric system becomes more isothermal in the horizontal with increasing oceanic heat transport. Main cause for this reduction of the global temperature gradient is the enhancement of convergence of latent heat fluxes. Convection spreads out from the deep tropics into the mid-latitudes leading to a large range of dynamic and thermodynamic changes. Warming of the troposphere in the mid- and high latitudes results in increased water vapour content. The results indicate that the investigated system becomes less efficient and more irreversible while planetary entropy production declines for increasing strength of the oceanic heat transport. The effect of thermalisation leading to the reduction of the efficiency of the system with increasing intensity of the ocean heat transport can be related to the decrease in the reservoir of the potential energy available for conversion in the Lorenz energy cycle (not show). The intensity of the Lorenz energy cycle declines by 1.3 Wm^{-2}, while material entropy production reduces by 9.8 $\mathrm{mWm}^{-2}\mathrm{K}^{-1}$ (both values for increasing $\Psi_{\max} = 0.0\,\mathrm{PW} \rightarrow \Psi_{\max} = 4.0\,\mathrm{PW}$).

The temperature difference between the warm (Θ^+) and the cold (Θ^-) heat reservoir decreases by 3.4 K in total for increasing oceanic heat transport. This is basically caused by an enhanced warming of the polar and subpolar low troposphere as well as tropo-

spheric cooling above the tropics. This warming is mainly due to intensified latent heat release by large-scale precipitation as corresponding heating patterns experience a shift from the mid- to high latitudes in the course of increasing the oceanic heat transport. This will lead to further warming due to the water vapour feedback (Herweijer et al., 2005; Barreiro et al., 2011).

By the result of reducing the planetary thermal difference the amount of available potential energy is decreased, leading to a decline in the transformation of kinetic energy. The intensity of the Lorenz energy cycle, thus, is reduced with the effect that the Hadley and the Ferrel circulation regimes experience a latitudinal shift and a decrease in intensity when increasing the heat transport in the ocean (not shown).

With increasing oceanic heat transport the surface temperature in the mid-latitudes rises. This surface heating destabilises the low-tropospheric air masses which respond with enhanced convective processes in the mid-latitude. As more heat is taken up by the ocean in the tropics and more heat is released in the mid-latitudes, heat is taken out of the Hadley cell regime, being most active in the tropics and subtropics, and is then released in the storm track area in the mid-latitudes (Rose and Ferreira, 2013).

As the atmosphere becomes more isothermal due to intensified mixing when increasing the oceanic heat transport, the strength of the Lorenz energy cycle as well as the efficiency decreases. This is consistent with the results in Lucarini et al. (2010) where higher CO_2 concentrations in the atmosphere result in global warming and smaller temperature differences in the atmosphere with a resulting decline in the efficiency as well as in the intensity of the Lorenz energy cycle.

When considering stronger oceanic transport, the climate system is characterised by a declining total material entropy production, while the degree of irreversibility increases, since the decrease in entropy production by frictional dissipation is more intense than the decrease in entropy generation due to sensible and, in particular, latent heat flux. The flux of latent heat contributes most to the material entropy production in the climate system. When increasing the heat transport in the ocean from 0.0 PW to 1.5 PW, material entropy production due to latent heat flux increases which can be explained by an outspread of convection from the deep tropics into the mid latitudes, while the maximum latent release is still located in the central tropics. When increasing the heat transport further, convective processes collapse in the deeps tropics and, thus, affecting evaporation intensities at tropical sea surface by reducing it. As a result, a decrease in material entropy production by latent heat fluxes can be noted from the increase of the oceanic heat transport larger than 2.0 PW.

In order to broaden the outlook in the field of study concerning the role of oceanic heat

transport, one could investigate the role of latitudinal location of the peak oceanic heat transport on macroscale thermodynamic properties. In the present set of experiments the peak oceanic transport was fixed at the latitude of 27°. The location of the peak can be adjusted by altering N in equation 8. This would complement the investigation by Rose and Ferreira (2013) and help understanding the properties of warm equable climates. One could apply the same theoretical framework as being used in this study. Another possible future line of investigation deals with studying planets with different astrophysical parameters, such as rotation rate, eccentricity, and obliquity, with the goal of contributing to the rapidly growing field of investigation of the atmosphere of exoplanets.

Acknowledgement

The authors acknowledge the support by the DFG Cluster of Excellence CLISAP. VL acknowledges the support of the FP7-ERC Starting Investigator Grant NAMASTE - Thermodynamics of the Climate System (No. 257037).

References

Ambaum, M. H. P. M. (2010). *Thermal physics of the atmosphere*, volume 1. Wiley. com.

Barreiro, M., Cherchi, A., and Masina, S. (2011). Climate Sensitivity to Changes in Ocean Heat Transport. *Journal of Climate*, 24(19):5015–5030.

Bjerknes, J. (1964). Atlantic air-sea interaction. *Advances in geophysics*, 10(1):82.

Covey, C. and Barron, E. (1988). The role of ocean heat transport in climatic change. *Earth-Science Reviews*, 24(6):429–445.

Enderton, D. and Marshall, J. (2009). Explorations of atmosphere-ocean-ice climates on an aquaplanet and their meridional energy transports. *Journal of the Atmospheric Sciences*, 66(6):1593–1611.

Fraedrich, K., Jansen, H., Kirk, E., and Lunkeit, F. (2005). The Planet Simulator: Towards a user friendly model. *Meteorologische Zeitschrift*, 14(3):305–314.

Goody, R. (2000). Sources and sinks of climate entropy. *Quarterly Journal of the Royal Meteorological Society*, 126(June):1953–1970.

Herweijer, C., Seager, R., Winton, M., and Clement, A. (2005). Why ocean heat transport warms the global mean climate. *Tellus A*, pages 662–675.

Johnson, D. R. (2000). Entropy, the Lorenz Energy Cycle and Climate. In *General Circulation Model Development: Past, Present and Future*, chapter 22, pages 659–720. Academic Press.

Kleidon, A. (2009). Nonequilibrium thermodynamics and maximum entropy production in the Earth system. *Naturwissenschaften*, 96(6):653–677.

Kleidon, A. and Lorenz, R. (2005). 1 Entropy Production by Earth System Processes. In *Thermodynamics and the Production of Entropy*. Springer DE.

Kuo, H.-L. (1965). On formation and intensification of tropical cyclones through latent heat release by cumulus convection. *Journal of the Atmospheric Sciences*, 22(1):40–63.

Lacis, A. A. and Hansen, J. (1974). A parameterization for the absorption of solar radiation in the earth's atmosphere. *Journal of the Atmospheric Sciences*, 31(1):118–133.

Laursen, L. and Eliasen, E. (1989). On the effects of the damping mechanisms in an atmospheric general circulation model. *Tellus A*, 41A(5):385–400.

Lorenz, E. (1955). Available potential energy and the maintenance of the general circulation. *Tellus*.

Lorenz, E. (1967). *The nature and theory of the general circulation of the atmosphere*. World Meteorological Organization, Geneva.

Louis, J. (1979). A parametric model of vertical eddy fluxes in the atmosphere. *Boundary-Layer Meteorology*, 7:187–202.

Lucarini, V. (2009). Thermodynamic efficiency and entropy production in the climate system. *Physical Review E*, 80(2):021118.

Lucarini, V., Blender, R., Pascale, S., Ragone, F., Wouters, J., and Herbert, C. (2014). Mathematical and Physical Ideas for Climate Science. *accepted for publication in Review of Geophysics*.

Lucarini, V., Fraedrich, K., and Lunkeit, F. (2010). Thermodynamics of climate change: generalized sensitivities. *Atmospheric Chemistry and Physics Discussions*, 10(2):3699–3715.

Lucarini, V., Fraedrich, K., and Ragone, F. (2011). New results on the thermodynamical properties of the climate system. *Journal of the Atmospheric Sciences*, 68:2438–2458.

Lucarini, V. and Pascale, S. (2014). Entropy production and coarse graining of the climate fields in a general circulation model. *Climate Dynamics*, 43(3-4):981–1000.

Lucarini, V. and Ragone, F. (2011). Energetics of climate models: Net energy balance and meridional enthalpy transport. *Reviews of Geophysics*, 49(2009):1–29.

Manabe, S. (1969). Climate and the ocean circulation: II. The atmospheric circulation and the effect of heat transfer by ocean currents. *Monthly Weather Review*, 97(11):775–805.

Ozawa, H., Ohmura, A., Lorenz, R., and Pujol, T. (2003). The second law of thermodynamics and the global climate system: a review of the maximum entropy production principle. *Reviews of Geophysics*, 41(4):1018.

Pauluis, O. and Held, I. (2002a). Entropy budget of an atmosphere in radiative-convective equilibrium. Part I: Maximum work and frictional dissipation. *Journal of the Atmospheric sciences*, 59(2):125–139.

Pauluis, O. and Held, I. (2002b). Entropy budget of an atmosphere in radiative-convective equilibrium. Part II: Latent heat transport and moist processes. *Journal of the Atmospheric sciences*, 59(2):140–149.

Peixoto, J. and Oort, A. (1992). *Physics of the Climate*. Springer-Verlag, New York.

Roeckner, E., Arpe, K., Bengtsson, L., Brinkop, S., Dümenil, L., Esch, M., Kirk, E., Lunkeit, F., Ponater, M., and Rockel, B. (1992). *Simulation of the present-day climate with the ECHAM model: Impact of model physics and resolution*. Max-Planck-Institut für Meteorologie Hamburg, Germany.

Romps, D. M. (2008). The dry-entropy budget of a moist atmosphere. *Journal of the Atmospheric Sciences*, 65(12):3779–3799.

Rose, B. E. J. and Ferreira, D. (2013). Ocean Heat Transport and Water Vapor Greenhouse in a Warm Equable Climate: A New Look at the Low Gradient Paradox. *Journal of Climate*, 26(6):2117–2136.

Sasamori, T. (1968). The radiative cooling calculation for application to general circulation experiments. *Journal of Applied Meteorology*, 7(5):721–729.

Slingo, A. and Slingo, J. M. (1991). Response of the National Center for Atmospheric Research community climate model to improvements in the representation of clouds. *Journal of Geophysical Research: Atmospheres*, 96(D8):15341–15357.

Stephens, G. L. (1978). Radiation profiles in extended water clouds. II: Parameterization schemes. *Journal of the Atmospheric Sciences*, 35(11):2123–2132.

Stephens, G. L. (1984). The parameterization of radiation for numerical weather prediction and climate models. *Monthly Weather Review*, 112(4):826–867.

Stone, P. (1978). Constraints on dynamical transports of energy on a spherical planet. *Dynamics of Atmospheres and Oceans*, 2:123–139.

Trenberth, K. E. and Caron, J. M. (2001). Estimates of meridional atmosphere and ocean heat transports. *Journal of Climate*, 14(16):3433–3443.

Wu, W. and Liu, Y. (2010). Radiation entropy flux and entropy production of the Earth system. *Reviews of Geophysics*, 48(2):1–27.